La$_2$MnVO$_6$ double perovskite: a structural, magnetic and X-ray absorption investigation†

Tapas Kumar Mandal,[a] Mark Croft,[b] Joke Hadermann,[c] Gustaaf Van Tendeloo,[c] Peter W. Stephens[d] and Martha Greenblatt[*a]

The synthesis, electron diffraction (ED), synchrotron X-ray and neutron structure, X-ray absorption spectroscopy (XAS) and magnetic property studies of La$_2$MnVO$_6$ double perovskite are described. Analysis of the synchrotron powder X-ray diffraction data for La$_2$MnVO$_6$ indicates a disordered arrangement of Mn and V at the B-site of the perovskite structure. Absence of super-lattice reflections in the ED patterns for La$_2$MnVO$_6$ supports the disordered cation arrangement. Room temperature time-of-flight (TOF) neutron powder diffraction (NPD) data show no evidence of cation ordering, in corroboration with the ED and synchrotron studies (orthorhombic $Pnma$, $a = 5.6097(3)$, $b = 7.8837(5)$ and $c = 5.5668(3)$ Å; 295 K, NPD). A comparison of XAS analyses of La$_2$TVO$_6$ with T = Ni and Co shows T^{2+} formal oxidation state while the T = Mn material evidences a Mn^{3+} admixture into a dominantly Mn^{2+} ground state. V-K edge measurements manifest a mirror image behavior with a V^{4+} state for T = Ni and Co with a V^{3+} admixture arising in the T = Mn material. The magnetic susceptibility data for La$_2$MnVO$_6$ show ferromagnetic correlations; the observed effective moment, μ_{eff} (5.72 μ_B) is much smaller than the calculated moment (6.16 μ_B) based on the spin-only formula for Mn^{2+} (d^5, HS) /V^{4+} (d^1), supportive of the partly oxidized Mn and reduced V scenario (Mn^{3+}/V^{3+}).

I. Introduction

Double perovskite oxides ($A_2BB'O_6$) continue to attract research interest, because of their unique electrical and magnetic properties that include metallic/half-metallic ferro/ferrimagnetism (HMFM), multiferroics, and colossal magnetoresistance (CMR).[1] The ordering of the transition metal ions (B and B') at the B-site of the perovskite structure is critical for the realization of these properties. Activity in double perovskite research has intensified since the discovery of room-temperature half-metallicity and tunneling-type magnetoresistance effect in Sr$_2$FeMoO$_6$ and Sr$_2$FeReO$_6$.

La$_2$MnVO$_6$ was predicted to be a half metallic antiferromagnet (HMAFM) by local spin-density functional calculations (DFT).[2] Following this report, Androulakis et al.[3] prepared La$_2$MnVO$_6$; however their compound was not a HMAFM, due to the apparent presence of high-spin Mn^{3+} and V^{3+}, and the absence of B-site order. Considering the negligible size difference between Mn^{3+} (0.645 Å)[4] and V^{3+} (0.64 Å), their ordering in the double perovskite structure is unexpected. Therefore, we have envisaged the synthesis of La$_2$Mn^{2+}V^{4+}O$_6$ to facilitate the

ordering of Mn^{2+} (0.83 Å) and V^{4+} (0.58 Å)[4] on the basis of size and charge considerations. Moreover, a high spin Mn^{2+} (d^5) and V^{4+} (d^1) would enhance B-site ordering and their anti-aligned spin orientation could possibly lead to a half-metallic ferrimagnet.

In the course of our investigation, the synthesis, structure and magnetic properties of La$_2$CoVO$_6$ and La$_2$NiVO$_6$ were reported by Holman et al.[5] Therefore this paper focuses on results of structural and magnetic investigations for La$_2$Mn^{2+}V^{4+}O$_6$ by powder X-ray, synchrotron and neutron diffraction, along with electron diffraction and SQUID magnetometry. The XAS studies, at the transition metal K edges of the series La$_2$TVO$_6$ (T = Mn, Co, Ni) presented, compare and contrast the formal oxidation states of Mn, Co, Ni and V as related to the intrinsic redox behavior of the transition metals in the system.

II. Experimental section

Polycrystalline samples of La$_2$TVO$_6$ (T = Mn Co, Ni) were synthesized by solid state reactions from high purity (purity ≥ 99.9 % Aldrich, or Alfa Aesar) stoichiometric quantities of La$_2$O$_3$, MnC$_2$O$_4$·2H$_2$O, CoO, NiO and VO$_2$. For the Co and Ni double perovskites the synthesis was carried out in sealed silica tubes with a slight modification of the literature procedure.[5] For this purpose, the starting materials were intimately ground (pre-synthesis and use of La$_2$NiO$_4$ and La$_2$CoO$_{4+\delta}$ was avoided), pressed into pellets and sealed in silica tubes under a dynamic vacuum of ∼1 × 10^{-8} Torr. The sealed ampoules were then heated at various temperatures and durations with a heating rate of 2 °C/min and after each step the products were examined for phase purity by powder X-ray diffraction (PXD). The products were thoroughly reground at intermediate steps. The synthesis of

[a]Department of Chemistry and Chemical Biology, Rutgers, The State University of New Jersey, 610 Taylor Road, Piscataway, NJ, 08854, USA. E-mail: martha@rutchem.rutgers.edu; Fax: +1 732 445 5312
[b]Department of Physics and Astronomy, Rutgers, The State University of New Jersey, 136 Frelinghuysen Road, Piscataway, NJ, 08854, USA
[c]Electron Microscopy for Materials Research (EMAT), University of Antwerp, Groenenborgerlaan 171, B-2020 Antwerp, Belgium
[d]Department of Physics and Astronomy, Stony Brook University, Stony Brook, NY, 11794-3800, USA
† This paper is part of a Journal of Materials Chemistry issue in celebration of the 75th birthday of C. N. R. Rao.

Table 1 Synthesis conditions and lattice parameters for La_2TVO_6 (T = Mn, Co, Ni)

Compound	Synthesis conditions	Lattice parameters (Å)[a]
La_2MnVO_6	850 °C/24h; 1050 °C/48h; 1125 °C/48h	$a = 5.6158(2)$, $b = 7.8807(3)$, $c = 5.5633(2)$
La_2CoVO_6	850 °C/96h; 1000 °C/72h; 1020 °C/72h	$a = 5.5476(6)$, $b = 7.8297(10)$, $c = 5.5381(7)$
La_2NiVO_6	950 °C/72h; 1050 °C/72h	$a = 5.5309(9)$, $b = 7.8043(14)$, $c = 5.5153(6)$

[a] Realistic estimates of precision of the lattice parameters would be several times larger.

phase pure La_2MnVO_6 was carried out in a reducing atmosphere. For this, stoichiometric quantities of intimately ground reagents were placed inside a tube furnace in an alumina boat and heated under a dynamic flow of 10 % H_2/90 % argon mixture, which was dried over anhydrous $CaSO_4$ and P_2O_5 before entering the furnace tube. The synthesis conditions for the formation of single-phase products are summarized in Table 1.

PXD patterns were recorded at room temperature on a Bruker D8-Advance diffractometer, in Bragg-Brentano geometry with CuK_α radiation, $\lambda = 1.5418$ Å, equipped with a SOL-X solid-state detector.

Synchrotron powder diffraction experiments on La_2MnVO_6 were performed at beam line X16C of the National Synchrotron Light Source at Brookhaven National Laboratory, equipped with a channel-cut Si(111) monochromator and Ge(111) analyzer. The sample was loaded in a quartz zero-background flat plate. A full pattern was taken at a wavelength of 0.69878(2) Å, for 2θ from 2° to 42° in steps of 0.01°, 2 sec per point. A series of scans at selected peak positions were collected in the neighborhood of the Mn-K edge, in steps of 0.01° for 40 sec per point. The Mn-K edge was located by measuring Mn Kα fluorescence from the sample using an Ampek Si diode detector, with a sample geometry identical to the diffraction measurements. Crystallographic refinements were performed using TOPAS software.[6]

Room temperature TOF NPD data for La_2MnVO_6 were collected on the Special Environment Powder Diffractometer (SEPD) at the Intense Pulsed Neutron Source (IPNS) at Argonne. The GSAS[7] program with the EXPGUI[8] interface was used for the crystallographic refinements from the NPD data.

Magnetic measurements were performed with a Quantum Design MPMS-*XL* superconducting quantum interference device (SQUID) magnetometer. Temperature dependent susceptibilities were measured at various applied magnetic fields (H) up to 5T in the temperature range 2 < T (K) < 400 after cooling the sample in zero magnetic field (zero-field cooled, ZFC) and also while cooling in the presence of the field (field-cooled, FC). Measurements of magnetization (M) as a function of H were made at 2 and 300 K over the magnetic field ranges $-50 \leq$ H (kOe) ≤ 50.

The Mn-, Co-, Ni- and V-K XAS measurements were collected simultaneously in both the transmission and fluorescence modes on powdered samples on beam line X-19A at the Brookhaven National Synchrotron Light Source.[9–19] A simultaneous standard

technique, in which the beam transmitted through the sample subsequently is used as the incident beam for the standard, was used to establish relative energy scale better than ± 0.05 eV. An ionization chamber in front of the sample monitored the sample-incident beam intensity. A second ionization chamber monitored the sample-transmitted and standard-incident beam intensities. The fluorescence intensities of both the sample and standard were measured with Canberra PIPS detectors.

The absolute energy calibration was set to the elemental K-edge (first inflection point) and the simultaneous standards were well studied oxide materials calibrated against the elemental standard. As is routinely done, the spectra had a linear background subtracted (determined over a ~80 eV interval below the edge), and were normalized to unity absorption step height across the edge. Here an average of the data in the ~50–200 eV range above the edge was used to set the normalization value.

Electron diffraction patterns were taken on a Philips CM20 transmission electron microscope. The samples were prepared by crushing the powder, dissolving it in ethanol and depositing drops of the solution on a holey carbon grid. Simulations of TEM images were made with the commercial software package JEMS.

III. Results and discussion

III.1. Synthesis and X-ray characterization

Single-phase polycrystalline La_2NiVO_6 and La_2CoVO_6 materials obtained as black powders were easily synthesized by the reactions described in the experimental section. Due to the apparently different redox chemistry of Mn and V compared to that of Co and Ni only the reducing atmosphere strategy adopted for the synthesis of La_2MnVO_6 yielded a pure phase. The PXD patterns for all the pure compounds prepared are shown in Fig. 1. Lattice parameter refinement of the laboratory PXD data (Table 1) for La_2NiVO_6 and La_2CoVO_6 is in fairly good agreement with that reported by Holman *et al.*[5] The PXD pattern of La_2MnVO_6 could be indexed satisfactorily in the orthorhombic *Pnma* space group with lattice parameters as listed in Table 1. The observed trend in the lattice parameters (Table 1) reflects the increasing
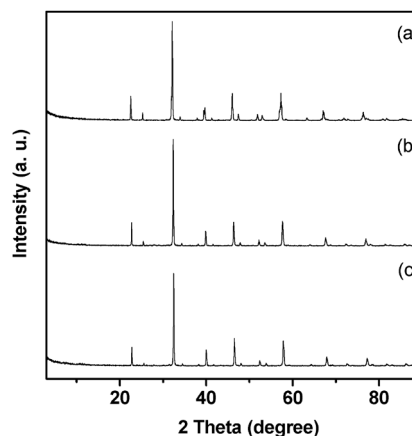

Fig. 1 Powder X-ray diffraction patterns of La_2TVO_6 (T = Mn, Co, Ni) double perovskites. (a) Mn, (b) Co and (c) Ni.

cation size in the series $Ni^{2+} < Co^{2+} < Mn^{2+}$ based on Shannon's[4] ionic radii values.

III.2. X-Ray absorption spectroscopy

The near-edge features at the K-edges of 3d transition metal, T(3d), compounds are due to transitions from the 1s to 4p states of the transition metal. These features are superimposed on an underlying step-feature due to the onset of 1s to continuum transitions. Multiple 4p features associated with different 3d configurations and with differing orbital orientations make interpretation of the near edge features difficult. Nevertheless the systematic energy shifts in the T(3d) K-edges, upon doping/ chemical changes, and the variation of feature intensities can

serve as indicators of charge transfer.[20] Most of the transition metal compounds discussed here manifest a sharp 4p-related peak at the edge which can be used to trace the chemical shift of the edge to higher energy with increasing valence.

III.2.a. T = Mn, Co and Ni: XAS results. The Mn-, Co-, and Ni-edges of the La_2TVO_6 (T = Mn, Co and Ni) double perovskites along with various standard compounds are shown in Fig. 2. Fig. 2a compares the Mn-K edge of La_2MnVO_6 to octahedrally coordinated perovskite based Mn-standards: the Mn^{2+} compounds Sr_2MnReO_6 and $LaSrMnSbO_6$;[11,12] the Mn^{3+} compounds $LaMnO_3$, Ca_2MnTaO_6, and Ca_2MnSbO_6;[10,12] and the Mn^{4+} compound $CaMnO_3$.[10] The spectra have been displaced vertically for clarity. For the standards selected the chemical shift
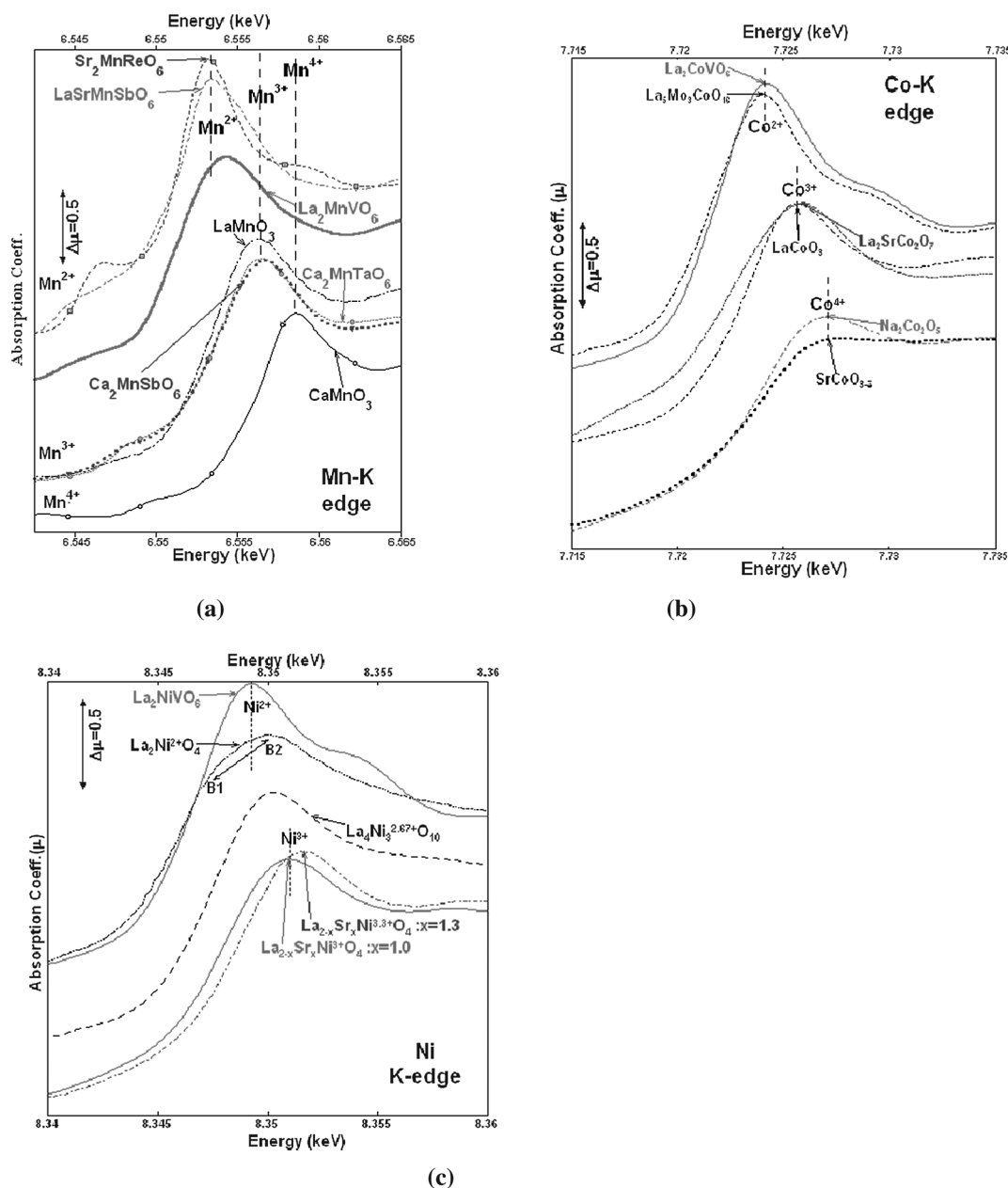

Fig. 2 X-Ray absorption spectra for La_2TVO_6 (T = Mn, Co and Ni) double perovskites along with representative T-K edge standards. (a) Mn-K edge, (b) Co-K edge, (c) Ni-K edge.

to higher energy with increasing valence can be seen in the shift of the energy of the peak-feature at the edge (see the valence-labeled dashed lines in the figure). Indeed in some of the Mn-perovskites the energy of this peak feature provides a sensitive quantitative measure of Mn-valence variations.[10] The chemical shift of the La_2MnVO_6 spectrum is clearly, albeit modestly, shifted up in energy relative to the Mn^{2+} standards (see Fig. 2a) but is much lower than the Mn^{3+} standards. Thus Mn appears to be mixed-valent [*i.e.* $Mn^{(2+\delta)+}$ with $\delta \sim 0.2$] in La_2MnVO_6.

In Fig. 2b the Co-K edge of La_2CoVO_6 sample is again compared with octahedrally coordinated standards: the Co^{2+} compound $La_5Mo_3CoO_{16}$;[13] the Co^{3+} compounds $LaCoO_3$ and $La_2SrCo_2O_7$;[14,15] and the Co^{4+} compounds $SrCoO_{3-\delta}$ and $Na_2Co_2O_5$.[15] The systematic chemical shift of the edge can, in these compounds, again be traced by the chemical shift of the peak-feature at the edge (again see the valence-labeled dashed lines in the figure). The strong hybridization present in the formally Co^{4+} compound standards leads to a broadening and diminution of the peak-feature at the edge. For our purposes the very sharp character and low energy of the peak feature (coincident with the Co^{2+} standard) clearly indicate the Co^{2+} valence state in La_2CoVO_6.

In Fig. 2c the Ni-K edge of La_2NiVO_6 is compared with octahedrally coordinated standards: the Ni^{2+} compound La_2NiO_4;[16,17] the mixed-valent $Ni^{2.67+}$ compound $La_4Ni_3O_{10}$;[16,17] the Ni^{3+} compound $La_{2-x}Sr_xNiO_4$ with x = 1.0; and the $Ni^{3.3+}$ compound $La_{2-x}Sr_xNiO_4$ with x = 1.3.[16,17] Again the systematic chemical shift of the edge can be traced by the chemical shift of the peak-feature at the edge (again see the valence-labeled dashed lines in the figure). In the case of the Ni^{2+} compound, La_2NiO_4, the distortion of the apical oxygens in the NiO_6 octahedra has been shown to lead to two separate peak features labeled B1 and B2 in Fig. 2c. The B1 and B2 features are respectively split down and up in energy so that the actual spectral peak at B2 lies above the peak energy expected for an undistorted octahedral environment. The apical-O distortion, and B1-B2 spectral splitting, have been shown to decrease with x in the $La_{2-x}Sr_xNiO_4$ compound series so that the peak feature provides a better valence-change marker in the x = 1.0 and 1.3 standard spectra shown in the figure.[16,17] The XAS results for La_2NiVO_6 are very similar to the Co isomorph discussed in the previous paragraph. Namely, the sharp structure and low energy shift of the peak feature clearly support the Ni^{2+} valence state in La_2NiVO_6.

III.2.b. V: XAS results. As illustrated in Fig. 3a the V-K edge lies in the range 10–15 eV below the La-L_3 edge making the XAS data analysis to estimate the V-valence variations more demanding. Fortunately the first inflection point and shoulder of the V-main edge are resolved from the very strong, higher energy "white line" peak at the La-L_3 edge. In Fig. 3a the numerical derivative (Fourier smoothed to remove statistical scatter) of the absorption coefficient spectra of La_2MnVO_6 can be seen to show a clear peak associated with the inflection point of the V-main edge rise absorption. Fig. 3b compares the derivative absorption spectra for $Eu^{2.5+}_2V^{3+}O_4$, and La_2TVO_6 with T = Ni, Co and Mn.[18,19] The derivative spectra of the T = Ni and Co compounds are essentially identical and their peaks are clearly shifted to higher energy, relative to the peak of the V^{3+}-standard $Eu^{2.5+}_2V^{3+}O_4$.[18,19] Consistent with the Ni^{2+} and Co^{2+} valence states determined above, the V-valence in these T = Ni and Co compounds is identified here as V^{4+} ($\sim V^{4+}$ in figure). It should be noted that the peak of the T = Mn, V-K derivative spectrum occurs at a dramatically lower energy compared to those of the Ni and Co spectra and at a higher energy than the V^{3+}-standard ($Eu^{2.5+}_2V^{3+}O_4$) spectral peak. Thus, while the above-determined Mn valence appeared to be mixed (and above 2+) in La_2MnVO_6, so too does the V-valence appeared mixed (and below 4+). Moreover, the XAS results directly evidence the expected conservation of the net valence of the {T-V} sites: with the low-valence T^{2+} being correlated with a mirror image high valence V^{4+} behavior in the T = Ni and Co compounds.

As indicated in the XAS results, the oxidation of Mn^{2+} is associated with a concomitant reduction of V^{4+} species and can be ascribed to an auto-redox mechanism operative in La_2MnVO_6 leading to $Mn^{2+} + V^{4+} \rightarrow Mn^{3+} + V^{3+}$ in contrast to stable M^{2+} and V^{4+} pairs in La_2TVO_6 (T = Co, Ni). Moreover, the enormous
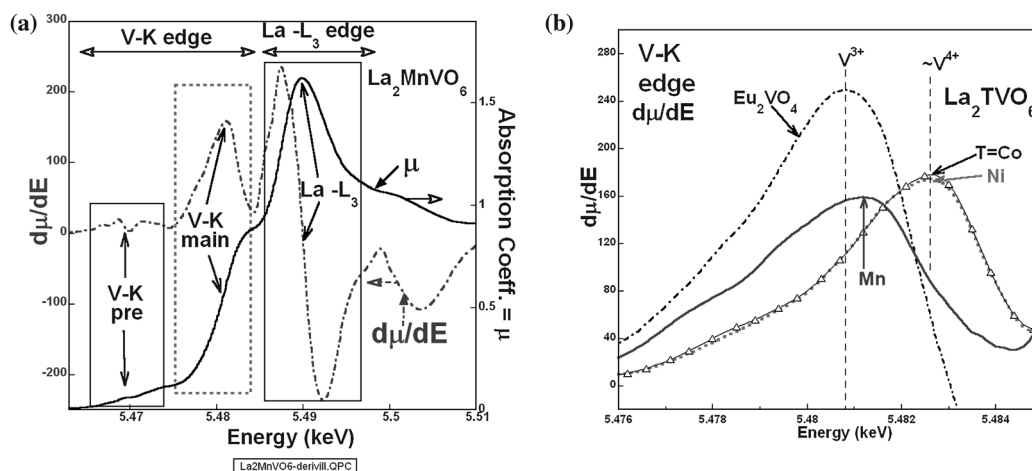

Fig. 3 (a) V-K X-ray absorption spectrum, and its derivative spectrum, for La_2MnVO_6 showing the Mn-K pre-edge and main-edge regions along with the prominent La-L_3 edge feature energies just above the Mn-edge onset. (b) V-K X-ray absorption derivative spectra for the standard compound $Eu^{2.5+}_2V^{3+}O_4$, and the La_2TVO_6 with T = Ni, Co and Mn compounds.

size mismatch between the six coordinated Mn^{2+} (0.83 Å) and V^{4+} (0.58 Å)[4] would also put the perovskite structure under considerable strain. Generally, the strain due to size mismatch between the A- and B-site cations in perovskites is relieved by the cooperative tilting of octahedra.[21] In La_2MnVO_6 the oxidation of Mn^{2+} to Mn^{3+} will result in a dramatic decrease of the ionic radii from 0.83 Å to 0.645 Å, thereby relieving the size strain. Concomitantly, the auto-redox process obliterates the charge and size difference of the B-site cations required for ordering in the double perovskite structure. The structural analysis (see later sections) indicates a disordered arrangement of the B-site cations in La_2MnVO_6. Therefore, we believe that a size-driven auto-redox, to relieve structural strain, is operative in La_2MnVO_6, and is responsible for the cation disordered double perovskite. Although, we are unaware of a previous report of size-driven internal redox in double perovskites, relief of structural strain *via* chemical oxidation of transition metal ions is known for K_2NiF_4-type oxides.[22]

III.3. Electron diffraction (ED)

Several tilt series with a total of 13 different selected area (SA) zone axis electron diffraction (ED) patterns were recorded, the main zones of which are shown in Fig. 4a. Convergent beam electron diffraction (CBED) patterns (Fig. 4b) and Kossel-Möllenstedt (K-M) patterns (Fig. 4c) were taken from the main zones. All reflections on the SAED and K-M ED, as well as the first order Laue zone (FOLZ) rings on the CBED patterns could be indexed with the cell parameters deduced from PXD. The reflection conditions, in agreement with all observed patterns, of SAED patterns are: hkl and $h0l$: no conditions; $hk0$: $h = 2n$; $0kl$: $k + l = 2n$; $h00$: $h = 2n$, $0k0$: $k = 2n$; and $00l$: $l = 2n$. The appearance of the reflections $h00$: $h \neq 2n$ and $00l$: $l \neq 2n$ on the [010] and those with $0k0$: $k \neq 2n$ on the [101] SAED pattern is due to double diffraction, as is evidenced by their absence on the [100] and [001] patterns. The reflection conditions $0k0$: $k = 2n$, $h00$: $h = 2n$ and $00l$: $l = 2n$ are further supported by the observation of Gjonnes-Moodie lines through all reflections $\neq 2n$ along these rows $h00$, $0k0$ and $00l$ on the K-M ED. The FOLZ reflections observed on the [001] and [110] patterns are also in agreement with the reflection conditions derived from ZOLZ reflections ([110] not separately shown here to limit figure size).

These reflection conditions leave only one possible extinction symbol: $Pn-a$, with two possible space groups, $Pnma$ (in agreement with PXD) and $Pn2_1a$. An attempt has been made to exclude $Pn2_1a$ by point group symmetry determination ($m2m$ and mmm) from the CBED patterns shown in Fig. 4b. The [101] CBED patterns show m perpendicular to b, which would indicate $Pnma$ as the correct space group. However, simulations of the CBED patterns for this material with the software package JEMS show hardly any difference between the two space groups. Apparently, the deviation from the symmetry in case of $Pn2_1a$ is too small to be discerned by the eye. The symmetry of the [010] pattern is $m2m$, which also agrees with both space groups.

III.4. Synchrotron powder X-ray diffraction

The synchrotron powder X-ray diffraction pattern of La_2MnVO_6 was readily indexed to an orthorhombic lattice. The
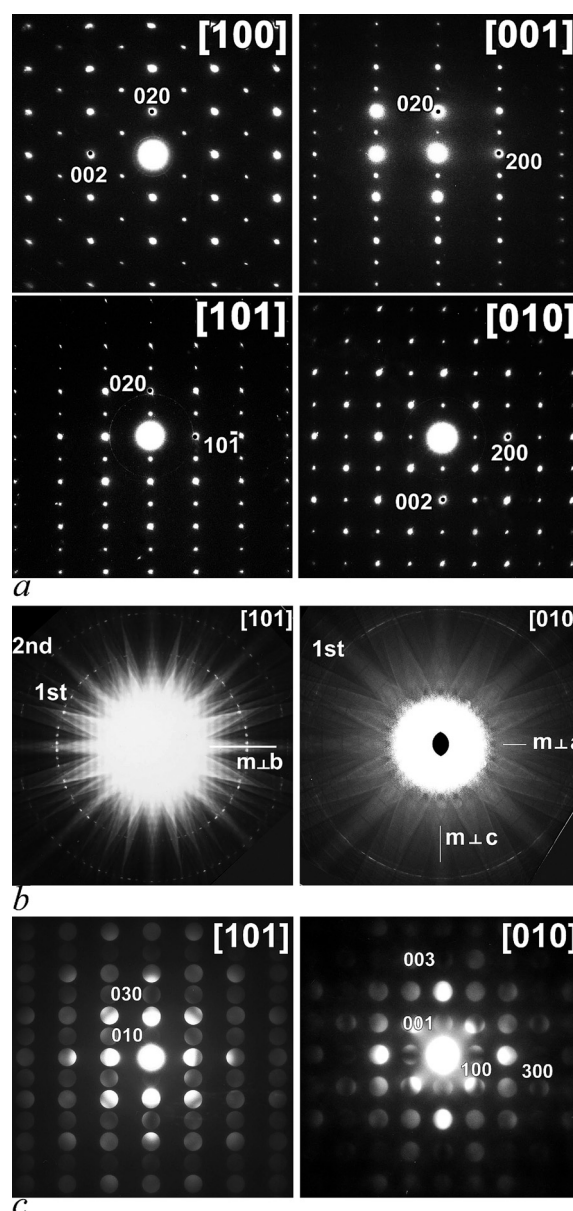

Fig. 4 ED patterns for La_2MnVO_6: (a) main zone selected area electron diffraction patterns; (b) CBED patterns of [101] and [010] at low camera length and (c) at higher camera length (K-M patterns).

structure was first refined for a simple perovskite (without B-site ordering) with the Glazer[23] tilt system $a^+b^-b^-$ with starting parameters in space group $Pnma$. The Rietveld refinement is shown in Fig. 5, and refinement and structural details are given in Table 2.

Part of the motivation for this work was to study the possibility of B-site ordering. Woodward has catalogued the possible space groups of ordered perovskites, and shown that the ordered form for this tilt system must be monoclinic.[21] This would be detectable in principle either through splitting of peaks as $\beta \neq 90°$, or by the observation of diffraction peaks forbidden in $Pnma$. A refinement in $P2_1/n$, shown in Table 2, is not significantly better than the disordered orthorhombic model (the deviation of the refined value of β from 90° is not regarded as significant.) Several peak positions which are allowed are shown
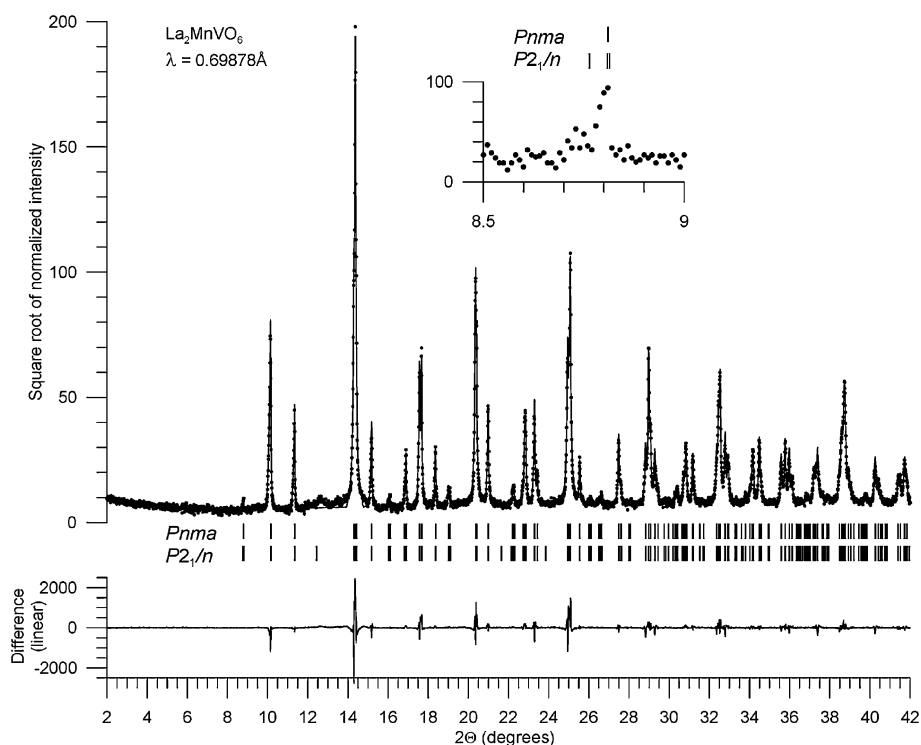
Fig. 5 Rietveld fit of synchrotron powder diffraction pattern of La_2MnVO_6 in space group *Pnma*. Tick marks also show allowed peaks in the corresponding $P2_1/n$ lattice. Note that the vertical scale of the main drawing is proportional to the square root of intensity, to better display the dynamic range of the data. Difference curve at the bottom is a linear scale. Inset shows the raw data in the neighborhood of the monoclinic (011) peak, which is essentially impossible to resolve in this data set.

Table 2 Refinement details of La_2MnVO_6 from synchrotron powder X-ray diffraction data. Numbers in parentheses are standard uncertainties from the least-squares refinement based on propagation of statistical errors alone. Realistic estimates of precision would be several times larger

	Orthorhombic	Monoclinic
Space group	*Pnma*	$P2_1/n$
a (Å)	5.6131(1)	5.6130(1)
b (Å)	7.8865(2)	5.5679(1)
c (Å)	5.5679(1)	7.8864(1)
β	90°	90.037(3)°
La	0.0375(2), ¼, 0.0068(3)	0.9935(4), 0.0375(1), 0.2492(9)
Mn	½, 0, 0 (50% occupied)	½, 0, 0
V	½, 0, 0 (50% occupied)	0, ½, 0
O1	0.988(2), ¼, 0.580(2)	0.203(5), 0.225(5), 0.953(3)
O2	0.287(2), 0.039(1), 0.285(2)	0.229(5), 0.199(5), 0.529(3)
O3		0.578(2), 0.012(2), 0.740(5)
R_{wp}	16.41%	16.28%
R_{exp}	7.62%	7.62%
χ^2	4.64	4.57
La–O distances	2.395(13) to 2.775(9)	2.40(1) to 2.82(3)
Mn–O distances	2.010(9) to 2.031(9)	2.10(4) to 2.13(3)
O–(Mn,V)–O angles	89.03(13) to 90.97(13)	87.3(8) to 92.7(8)

in the refinement in Fig. 5, but none of them is observed. However, since the potential ordering is between elements differing by only two electrons, the amplitude of an ordering peak would be expected to be very weak.

In order to enhance the signal from ordered *B*-site ions, we performed a resonant diffraction experiment, in which the region of the monoclinic (011) peak was scanned for X-ray wavelengths near the Mn-K edge. The atomic scattering factor for X-rays is generally written as f(sinθ/λ) + f′(λ) + if″(λ), where f′ changes by

several electrons in the vicinity of the K edge. This allows us to enhance the X-ray contrast between the V and Mn atoms (the V-K edge might have been more favorable, but it was inaccessible to the tuning range of the X-ray monochromator). Fig. 6 shows the fluorescence signal as a function of X-ray wavelength. The energy resolution of the monochromator and the core-hole lifetime are modeled by a Lorentzian of full-width at half-maximum of 0.0016 Å (5.6 eV). The real part of the anomalous scattering amplitude, f′(λ) tabulated by Sasaki,[24] was numerically
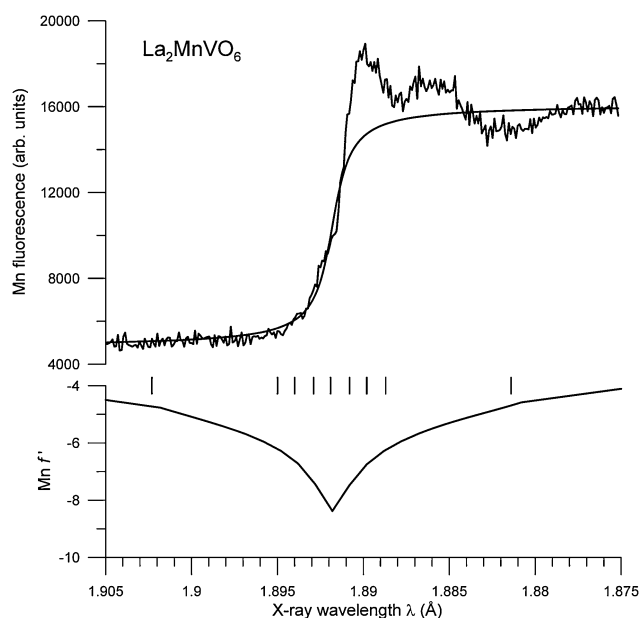
Fig. 6 Fluorescence signal from La_2MnVO_6 at the Mn-K edge. The smooth curve in the upper panel is the convolution of a step function with a Lorentzian. The lower trace is the computed anomalous atomic scattering factor for Mn, shifted to the observed edge wavelength and convoluted with the same Lorentzian. Tick marks indicate wavelengths where powder diffraction scans of the region of the monoclinic (011) peak were collected.
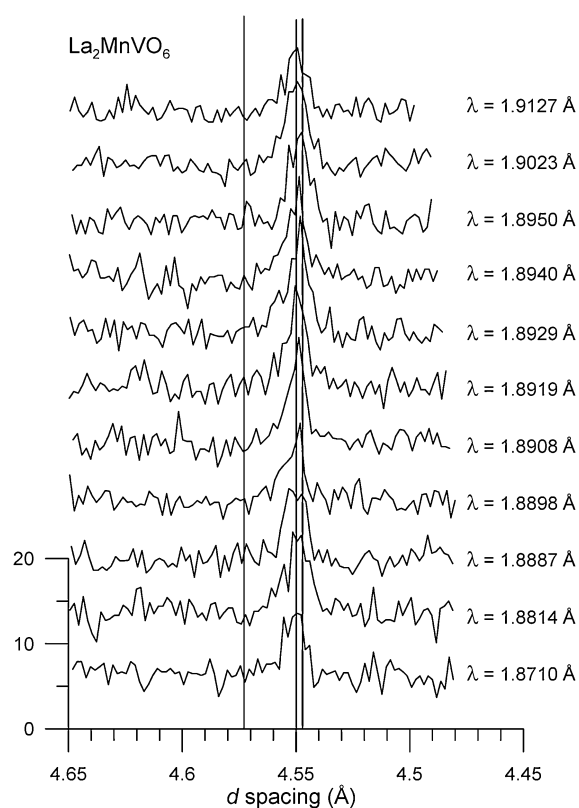

Fig. 7 Powder X-ray diffraction patterns in the neighborhood of the presumed monoclinic (011) peak, collected at various X-ray wavelengths. The vertical lines indicate positions of monoclinic (011), (10−1), and (101) reflections; the orthorhombic (011) reflection is coincident with the latter two monoclinic reflections.

convoluted with the same Lorentzian to obtain an estimate of the anomalous scattering amplitude of the Mn ions subject to the same influence of core-hole lifetime and energy resolution, illustrated in Fig. 6.

We then collected diffraction patterns in the region of one peak that would have a contribution from the difference of ions in the B sites, the presumed monoclinic (011) reflection. The same scans covered the nearby monoclinic (10−1) and (101) reflections, which are essentially coincident with the (allowed) orthorhombic (011); all of these are allowed reflections whether or not there is B-site ordering. The scans are shown in Fig. 7. In this range, the f′ of vanadium is −0.7, so the difference of effective scattering factors of V minus Mn ranges from 2.1 to 5.6. At a maximum, this leads to a computed ratio $I_{011}/(I_{10\text{-}1} + I_{101}) = 25\%$. Since no trace of the monoclinic (011) reflection is ever seen, we conclude that there is no B-site ordering in this material. We mention in passing that the same technique has been successfully applied to observe B-site ordering in $La_{1.5}Gd_{0.5}MnNiO_6$.[25]

III.5. Neutron powder diffraction

Following the synchrotron X-ray structure, the Rietveld refinement of the room temperature NPD data was carried out in the characteristic $Pnma$ space group for the B-site disordered double perovskite with the same $a^+b^-b^-$ tilt system. All the reflections could be indexed adequately in $Pnma$ and the profile analysis allowed a very good description of the peak shapes. A trial refinement for the ordered arrangement of the Mn and V within the same tilt system in the $P2_1/n$ space group did not result in a superior fit over the cation disordered $Pnma$. The reliability factors for the refinement in $Pnma$ ($wR_p = 5.16\%$, $R_p = 3.78\%$, χ^2

= 1.78) are comparable to those for $P2_1/n$ ($wR_p = 5.46\%$, $R_p = 3.93\%$, $\chi^2 = 1.78$). On the basis of slightly better profile matching we accepted the $Pnma$ as the preferred space group consistent with the SPXD studies. The experimental, calculated and difference NPD profiles for the $Pnma$ space group are shown in Fig. 8 and the refined structural parameters are listed in Table 3. The crystal structure based on the refined atomic coordinates is also shown in Fig. 8. The octahedral tilt angles calculated from the Mn/V–O–Mn/V bond angles are found to be 12.56 and 12.61°. The Mn/V–O bond distances vary from 2.008(1) to 2.041(1) Å with an average distance of 2.023(1) Å.

III.6. Magnetic properties

The temperature dependences of the magnetic susceptibility (both FC and ZFC) and the inverse susceptibility (FC only) data at different applied fields for La_2MnVO_6 are shown in Fig. 9. Below ≈ 80 K the magnetic susceptibility (see Fig. 9a and inset) starts to increase rapidly followed by an AFM-like transition at ≈ 20 K. The ZFC and FC susceptibility diverge only at or near the transition in low magnetic fields, but overlap at high magnetic field strengths. The high temperature susceptibility is Curie-Weiss like with a positive, FM Weiss constant (see the inverse susceptibility plot in Fig. 9b). The 1000 Oe FC data are representative of all the high temperature data and yield a Curie-Weiss fit (over the 300–400 K range) with a Weiss
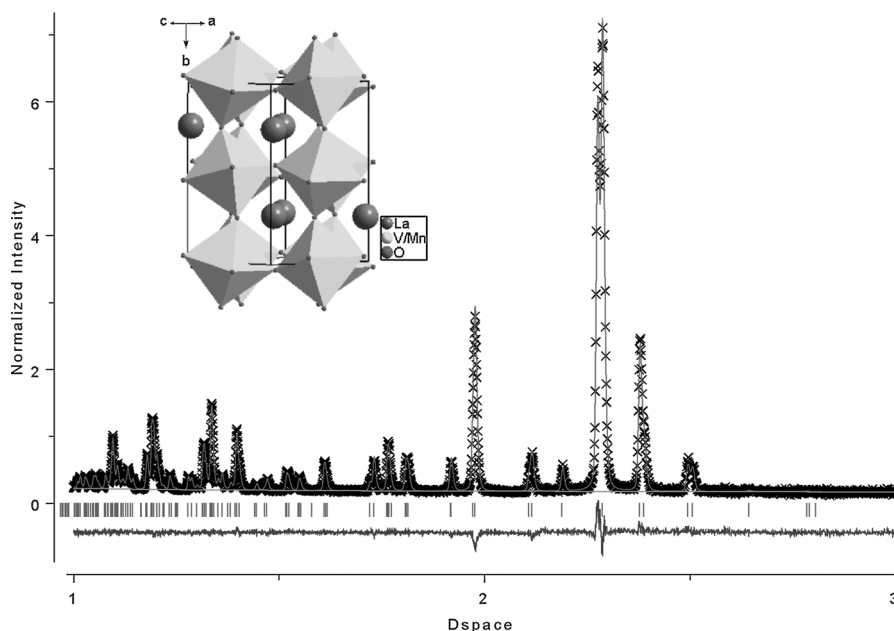
Fig. 8 Observed (crosses), calculated and difference profiles for the room temperature TOF-NPD data of La_2MnVO_6. The tick marks represent the Bragg positions.

Table 3 Structural parameters for La_2MnVO_6 from the NPD data at 295 K[a]

Atom	Wyckoff position	x	y	z	$10^2 U_{iso}$ ($Å^2$)	occ
La	4c	0.0369(1)	0.25	0.0076(2)	0.79(4)	1.0
Mn	4b	0.5	0.0	0.0	0.30(6)	0.5
V	4b	0.5	0.0	0.0	0.30(6)	0.5
O1	4c	0.9838(2)	0.25	0.5775(3)	1.08(5)	1.0
O2	8d	0.2897(1)	0.0409(1)	0.2861(1)	1.09(5)	1.0

[a] Space group: *Pnma* (No. 62); $a = 5.6106(1)$, $b = 7.8845(3)$ and $c = 5.5673(1)$ Å; $\chi^2 = 1.78$, $wR_P = 5.16\%$ and $R_P = 3.78\%$.

temperature $\theta_W \approx 33$ K, indicating weak ferromagnetic interactions.

The fitted paramagnetic Curie constant corresponds to an effective magnetic moment of 5.72 μ_B. The calculated spin-only formula moments for a $Mn^{2+}(d^5$, HS)-$V^{4+}(d^1)$ couple and $Mn^{3+}(d^3$, HS)-$V^{3+}(d^2)$ couple are 6.16 μ_B and 5.65 μ_B, respectively. In view of the XAS evidence for intermediate valence states on both the Mn and V sites in this compound, the intermediate moment is qualitatively not surprising, however quantitatively a value somewhat closer to the $Mn^{2+}(HS)$-V^{4+} couple would have been anticipated from the XAS results. The significant ferrimagnetic correlations in the system would be consistent with both the observed positive Weiss constant and the reduced paramagnetic Curie moment. The Mn^{2+}–O–V^{4+} and Mn^{3+}–O–V^{3+} AFM super-exchange pathways would both result in ferrimagnetic interactions.

The magnetization data at 300 K show pure paramagnetic behavior while at 5 K there is significant non-linearity with a small hysteresis (Fig. 10). The highest moment obtained at 5 T is 2.26 μ_B at 5 K and the system is still not saturated at this field. The positive Weiss temperature together with the hysteretic magnetization further supports the ferrimagnetic scenario.
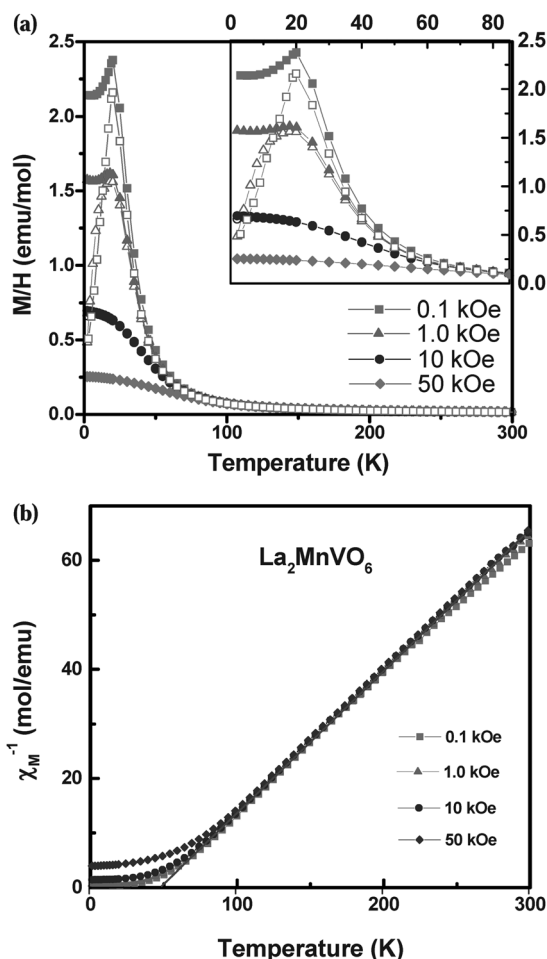

Fig. 9 (a) Magnetic susceptibility vs. temperature plots for La_2MnVO_6 at different applied magnetic fields; open symbols are ZFC, and closed symbols are FC measurements. Inset shows an expanded view of the low temperature region. (b) The field cooled (FC) inverse molar susceptibility vs. temperature plots.
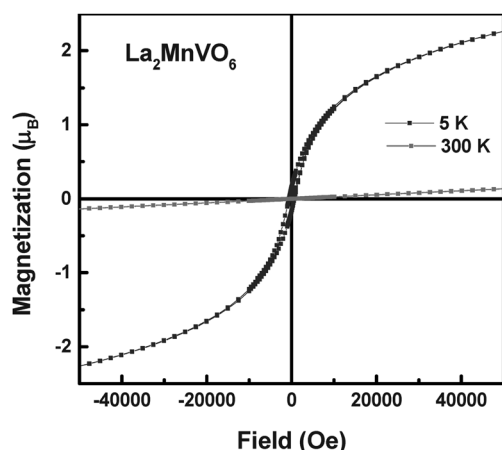
Fig. 10 Magnetization vs. field data for La_2MnVO_6 at 5 and 300 K.

IV. Conclusion

La_2MnVO_6 formed in the double perovskite structure with a disordered arrangement of Mn and V at the *B*-site as evidenced by ED, SPXD and NPD studies. The XAS results support valence mixing on both the Mn and V sites supporting an auto-redox mechanism operating in La_2MnVO_6 leading to $Mn^{2+} + V^{4+}$ → $Mn^{3+} + V^{3+}$. This stands in contrast to the XAS results on the La_2TVO_6, T = Co and Ni, compounds where a sharp T^{2+}/V^{4+} valence distribution is observed. This observation lends further support for the auto-redox occurring in La_2MnVO_6, which could relieve the strain due to size mismatch between Mn^{2+} (0.83 Å) and V^{4+}(0.58 Å) in the lattice, and explain the absence of order in La_2MnVO_6.

Acknowledgements

References

1 (*a*) K.-I. Kobayashi, T. Kimura, H. Sawada, K. Terakura and Y. Tokura, *Nature (London)*, 1998, **395**, 677; (*b*) K.-I. Kobayashi, T. Kimura, H. Sawada, K. Terakura and Y. Tokura, *Phys. Rev.*, 1999, **B59**, 11159; (*c*) H.-Y. Hwang, S.-W. Cheong, N. P. Ong and B. Battlogg, *Phys. Rev. Lett.*, 1996, **77**, 2041.
2 W. E. Pickett, *Phys. Rev.*, 1998, **B57**, 10613.
3 J. Androulakis, N. Katsarakis and J. Giapintzakis, *Solid State Commun.*, 2002, **124**, 77.
4 R. D. Shannon, *Acta Crystallogr.*, 1976, **A32**, 751.
5 K. L. Holman, Q. Huang, T. Klimczuk, K. Trzebiatowski, J. W. G. Bos, E. Morosan, J. W. Lynn and R. J. Cava, *J. Solid State Chem.*, 2007, **180**, 75.
6 Bruker AXS (2005), *TOPAS V3: General profile and structure analysis software for powder diffraction data -User's Manual*, Bruker AXS, Karlsruhe, Germany.
7 A. C. Larson, R. B. Von Dreele, *General Structure Analysis System (GSAS)*, Los Alamos National Laboratory Report LAUR, 2000, **86**, 748.
8 B. H. Toby, *J. Appl. Crystallogr.*, 2001, **34**, 210.
9 J. M. Tranquada, S. M. Heald, A. R. Moodenbaugh, G. Liang and M. Croft, *Nature (London)*, 1989, **337**, 720.
10 M. Croft, D. Sills, M. Greenblatt, C. Lee, S.-W. Cheong, K. V. Ramanujachary and D. Tran, *Phys. Rev*, 1997, **B55**, 8726.
11 G. Popov, M. Greenblatt and M. Croft, *Phys. Rev.*, 2003, **B67**, 024406.
12 T. Mandal, A. Abakumov, M. Lovanov, V. Poltavets, M. Croft, J. Stalick and M. Greenblatt, *Chem. Mater.*, 2008, **20**, 4653.
13 K. Ramanujschary, S. Lofland, W. McCarroll, T. Emge, M. Greenblatt and M. Croft, *J. Solid State Chem.*, 2002, **164**, 60.
14 J. E. Sunstrom IV, M. Greenblatt and M. Croft, *J. Solid State Chem.*, 1998, **139**, 388.
15 G. Veith, R. Chen, Popov M. Greenblatt, M. Croft and I. Nowik, *J. Solid State Chem.*, 2002, **166**, 292.
16 A. Sahiner, M. Croft, S. Gua, I. Perez, Z. Zhang, M. Greenblatt, P. Metcalf, H. Johns and G. Liang, *Phys. Rev.*, 1995, **B51**, 5879.
17 A. Sahiner, M. Croft, Z. Zhang, M. Greenblatt, I. Perez, P. Metcalf, H. Jhans, G. Liang and Y. Jeon, *Phys. Rev.*, 1996, **B53**, 9745.
18 K. V. Ramanujachary, J. Sunstrom IV, I. Fawcett, P. Shunk, M. Greenblatt, M. Croft, I. Novick, R. H. Herber and S. Khalid, *Mater. Res. Bull.*, 1999, **34**, 803.
19 I. Nowik, R. Herber, I. Felner, K. V. Ramanujachary, J. E. Sunstrom IV, I. Fawcett, P. Shunk, M. Greenblatt and M. Croft, *Phys. Rev.*, 1999, **B59**, 8732.
20 Q. Qian, T. A. Tyson, C. C. Kao, J. P. Rueff, F. M. F. de Groot, M. Croft, S. W. Cheong, M. Greenblatt and M. A. Subramanian, *J. Phys. Chem. Solids*, 2000, **61**, 457.
21 P. M. Woodward, *Acta Crystallogr.*, 1997, **B53**, 32.
22 J. Rodríguez-Carvajal, M. T. Fernández-Díaz and J. L. Martínez, *J. Phys.: Condens. Matter*, 1991, **3**, 3215.
23 A. M. Glazer, *Acta Crystallogr.*, 1972, **B28**, 3384.
24 S. Sasaki, "*Numerical Tables of Anomalous Scattering Factors Calculated by the Cromer and Liberman's Method*," KEK Report, 1989, 88.
25 A. Huq *et al.*, in preparation.